Phase diagram of calcium at high pressure and high temperature

S. Anzellini,[1,*] D. Errandonea,[2] S. G. MacLeod,[3,4] P. Botella,[5] D. Daisenberger,[1] J. M. De'Ath,[3] J. Gonzalez-Platas,[6] J. Ibáñez,[7] M. I. McMahon,[4] K. A. Munro,[4] C. Popescu,[8] J. Ruiz-Fuertes,[9] and C. W. Wilson[3]

[1]*Diamond Light Source Ltd., Diamond House, Harwell Science Campus, Didcot, Oxfordshire OX11 0DE, United Kingdom*
[2]*Departamento de Física Aplicada-Instituto de Ciencia de Materiales, Matter at High Pressure (MALTA) Consolider Team, Universidad de Valencia, Edificio de Investigación, C/Dr. Moliner 50, Burjassot, 46100 Valencia, Spain*
[3]*AWE, Aldermaston, Reading RG7 4PR, United Kingdom*
[4]*SUPA, School of Physics and Astronomy, and Centre for Science at Extreme Conditions, The University of Edinburgh, Edinburgh, EH9 3FD, United Kingdom*
[5]*Luleå University of Technology, Department of Engineering Sciences and Mathematics, Luleå, 971 87, Sweden*
[6]*Departmento de Física, Universidad de La Laguna, Avda. Astrofísico Fco. Sánchez s/n, E-38206 La Laguna, Tenerife, Spain*
[7]*Institute of Earth Sciences Jaume Almera, CSIC, 08028 Barcelona, Spain*
[8]*CELLS-ALBA Synchrotron Light Facility, 08290 Cerdanyola, Barcelona, Spain*
[9]*DCITIMAC, MALTA Consolider Team, Universidad de Cantabria, 39005 Santander, Spain*

(Received 13 July 2018; published 30 August 2018)

Resistively heated diamond-anvil cells have been used together with synchrotron x-ray diffraction to investigate the phase diagram of calcium up to 50 GPa and 800 K. The phase boundaries between the Ca-I (fcc), Ca-II (bcc), and Ca-III (simple cubic, sc) phases have been determined at these pressure-temperature conditions, and the ambient temperature equation of state has been generated. The equation of state parameters at ambient temperature have been determined from the experimental compression curve of the observed phases by using third-order Birch-Murnaghan and Vinet equations. A thermal equation of state was also determined for Ca-I and Ca-II by combining the room-temperature Birch-Murnaghan equation of state with a Berman-type thermal expansion model.

DOI: 10.1103/PhysRevMaterials.2.083608

I. INTRODUCTION

In its pure form, the Group II alkaline-earth-element calcium (Ca) has a dull silvery metal appearance, although it is never found in this state in nature as a consequence of its inherent instability in air. Ca is a constituent of many minerals such as calcite [1], gypsum [2], and fluorite [3]. It is an essential component in bone formation [4], and blood and soft-tissue function [5]. It is also found in a wide variety of applications, in compound or alloy form, in the food, pharmaceutical, medical, and chemical industries [6].

Ca is known to be stable at ambient conditions in the face-centered cubic (fcc) structure [7]. The crystal structure of Ca and other Group II elements, at ambient conditions, are correlated with the occupation of their d-electron levels [7]. Under compression, these elements were predicted to transform from densely packed structures to open-packed low-symmetry structures [7]. Such unexpected behavior has generated much interest in the study of the underlying physical mechanisms [7–9]. In the case of Ca, with increasing pressure, the 3d electron energy levels move downward, close to the Fermi level, and as a consequence of an sp-d electron transfer, the d character of the valence band is increased [7,8]. With a broadening of the core bands dominating, the structural sequence for Ca at 0 K has been calculated to be fcc → body-centered cubic (bcc) → hexagonal close-packed (hcp) [7]. In contrast, Ahuja *et al.*, using a full-potential linear muffin-tin orbital method, found the transition to be from bcc to another open structure, simple cubic (sc), with an associated large volume collapse [8]. However, in a more recent theoretical work, carried out using molecular dynamics, the existence of two solid post-bcc phases with orthorhombic *Cmcm* and *Pnma* structures has been proposed instead of the sc structure [9].

Several experimental compression studies have been performed on Ca at room temperature (RT). In particular, prior to the study of Ahuja *et al.* [8], it was found using diamond-anvil cells (DACs) and x-ray diffraction (XRD) that Ca-I (fcc) transforms into Ca-II (bcc) at 19.5 GPa, with a volume change $\Delta V/V$ of 2%, and then into Ca-III (sc) at 32 GPa with a volume change of 8% [10]. The Ca-III phase is stable up to 113 GPa, whereupon it transforms into the Ca-IV phase, and then a further transformation into the Ca-V phase takes place above 139 GPa [11]. The space groups of the Ca-IV and Ca-V phases were later clarified as tetragonal $P4_12_12$ and orthorhombic *Cmca*, respectively [12,13]. Under further compression, the Ca-V phase (*Cmca*) transforms to the orthorhombic Ca-VI structure (space group *Pnma*) at 158 GPa [14]. A possible host-guest structure was reported at 210 GPa [15], although it has been suggested that the structure of this Ca-VII phase could be a 32-atom tetragonal cell ($tI32$) [16]. The Ca-VII phase is stable to 241 GPa, the highest pressure achieved experimentally in Ca [15].

*simone.anzellini@diamond.ac.uk

Calcium has been also studied under compression at low temperature (LT). A superconducting behavior was reported for Ca at 50 GPa and 1.2 K with the superconducting transition temperature increasing linearly with pressure and reaching one of the highest critical temperatures (25 K) among the elements of the periodic table [11,15].

In contrast with RT and LT studies, very few combined high-pressure high-temperature (HP-HT) experiments have been performed on Ca [17–19] and none of these studies have utilized XRD to unambiguously determine the observed crystal structures. At ambient pressure, Ca-I (fcc) is known to transform into a bcc phase near 730 K. It has been speculated that this HT bcc phase is the same Ca-II (bcc) phase obtained at RT at 19.5 GPa. However, no direct evidence showing that the HT bcc phase and Ca-II (bcc) are the same phase has yet been reported.

In an early HP-HT study, a piston-cylinder apparatus was used to generate pressures up to 4 GPa and the fcc to bcc solid-solid phase boundary and melting curve up to 1500 K were determined using differential thermal analysis [17,18]. Temperatures were measured using a chromel-alumel thermocouple, but no corrections were made for the effects of pressure on the temperature given by the thermocouple. The melting curve of Ca was also studied up to 80 GPa and 3000 K in a lab-based DAC experiment using single-sided laser heating to induce melting [19]. Pressures were determined using the ruby R_1 fluorescence method [20]. Melting of the sample surface was probed using the laser-speckle technique [21] and surface temperature was determined using spectral radiometry [22,23]. The unusual melting curve, which flattens out at ∼1500 K between 5 and 32 GPa, suggests that Ca is melting from the Ca-II (bcc) phase, supporting the hypothesis that HT-bcc Ca and HP Ca-II (bcc) are the same phase [19]. Furthermore, the existence of a Ca-II-Ca-III-liquid (bcc-sc-liquid) triple point located at 32 GPa and 1550 K has been proposed [19]. Above 32 GPa, the slope of the melt curve increases dramatically $[(dT/dP) \sim 96\,\mathrm{K\,GPa^{-1}}]$ until at around 45 GPa and 2750 K the melt slope almost flattens $[(dT/dP) \sim 3\,\mathrm{K\,GPa^{-1}}]$ [19].

The results summarized above indicate that there are many open questions on the structural behavior of Ca under HP-HT conditions. This suggests that additional efforts are needed to accurately determine the HP-HT phase diagram. Thus, we have performed a series of angle-dispersive powder XRD (AD-XRD) HP-HT experiments using DACs and resistive heating to study Ca up to 50 GPa and 800 K. Here, we present thermal equations of state (EOSs) for Ca-I, Ca-II, and Ca-III, and determine the boundaries between these phases. The results are discussed with reference to the previous information available in the literature [8–25].

II. EXPERIMENTAL SETUP

Ten membrane DACs were prepared with 300-μm-diameter culet anvils. Three series of AD-XRD experiments were performed: two at the Materials Science and Powder Diffraction beamline BL04 at the ALBA synchrotron [26], and one at the Extreme Conditions beamline I15 at the Diamond Light Source (DLS) synchrotron.

For the two sets of experiments performed at ALBA, four DACs were prepared with rhenium gaskets and two DACs with stainless-steel gaskets. For the experiment performed at DLS, four DACs were prepared with rhenium gaskets. In all cases the Ca loadings were performed under an inert atmosphere to prevent sample oxidation or other possible chemical reactions. Samples were cut from a piece of 99% purity Ca, sourced from Goodfellow. Main impurities are Al (800 ppm) and Mg (1000 ppm), according to the information provided by the vendor. For the first group of experiments at ALBA, the Ca samples were loaded together with a small piece of 3-μm-thick Au foil, which acted as the pressure standard. No pressure-transmitting medium was used. In these experiments, at HT we detected a chemical reaction between the rhenium and steel gaskets and Ca after the fcc-bcc phase transition was observed, which not only resulted in the deterioration of sample, but caused the gaskets to collapse. This suggests a change in the electronic structure of Ca in the bcc phase, which enhances the chemical reactivity of Ca. The subsequent experiments at ALBA and Diamond differed from the first runs at ALBA in that oven-dried KCl disks were loaded as the pressure medium and to isolate the sample from the gaskets and diamonds. Au foil was again added as the pressure marker. No evidence of chemical reactions was detected in these experiments up to 50 GPa and 800 K.

In the high-temperature experiments the DACs were heated using 240-V Watlow coiled-cable heaters, which were wrapped around the outside of each DAC, and which can operate continuously at a power density greater than $4.65\,\mathrm{W\,cm^{-2}}$. These heaters are capable of inducing temperatures of up to 900 K in samples. For temperature measurement, K-type thermocouples, with an accuracy <0.4% were attached to the piston of the DAC, close to one of the diamond anvils. The DAC was housed inside a dedicated water-cooled vacuum vessel which was evacuated using a rotary-backed turbo pump. An evacuated environment prevents oxidation of the diamonds at high temperatures and removes the effects of convective heating. Typically, vacuum pressures of $\sim 10^{-4}$–10^{-5} mbar were achieved within the vessel during the course of the experiments. Water cooling ensured the vessel remained cool (approximately at RT) relative to the heated DAC and any thermally induced movement of the sample with respect to the x-ray beam was thus minimized. This apparatus has been successfully used in previous HP-HT AD-XRD DAC experiments at different synchrotron facilities [27,28]. The sample pressure was determined from the XRD patterns of Au and KCl according to the EOSs of Dorogokupets and Dewaele [29] and Dewaele *et al.* [30], respectively. The pressure difference between both pressure standards was always smaller than 1 GPa.

Before each heating run, the sample was pressurized at RT to approximately 3 GPa and then heated up while collecting XRD data. Once the target temperature was reached, isothermal compressions were performed, and XRD patterns were collected every 1–2 GPa using an SX165 Rayonix charge-coupled device camera at ALBA and a Mar345 image plate detector at DLS. XRD patterns were collected on both beamlines using a monochromatic beam with a wavelength of 0.4246 Å and at a sample-to-detector distance of ∼320 mm on I15 and ∼180 mm on BL04. The detector geometry was calibrated with a LaB_6 standard in each case. The raw AD-XRD images were integrated using the DIOPTAS software suite [31] and the

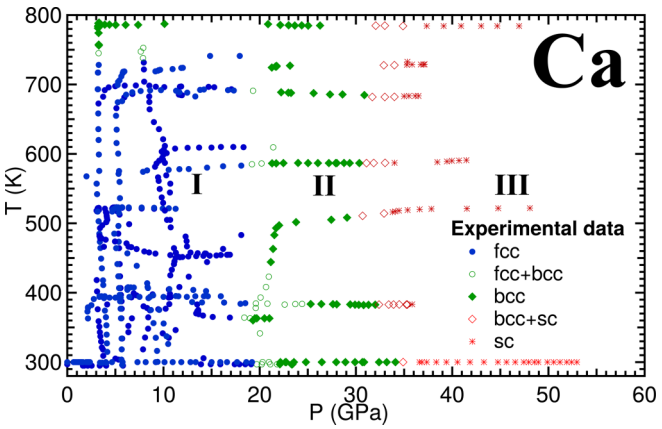

FIG. 1. Phase diagram of Ca, as obtained in the present study. The experimental points are represented by circles, diamonds, and asterisks. Solid symbols represent pure phases whereas empty symbols represent phase coexistence.

resulting one-dimensional (1D) profiles were analyzed by Le Bail fitting using the TOPAS program [32].

III. RESULTS AND DISCUSSION

A. Phase diagram

The structural evolution of Ca has been investigated up to 53 GPa and 800 K as summarized in Fig. 1 where the stability regions of the different Ca phases can be seen. Notice that these regions do not necessarily describe the thermodynamically stable fields since usually, first-order phase transitions (like those here observed) can be strongly affected by kinetic barriers [33]. Therefore, the phase boundaries experimentally determined in the present study might correspond to kinetic phase boundaries [34].The isotherm collected at around 800 K (from 3 to 27 GPa) and the HP-HT experiments performed from 20 to 30 GPa (from 300 to 800 K) confirm that the Ca-II (bcc) phase and the ambient pressure HT bcc phase of Ca are quite likely one and the same. The transformation of fcc Ca into bcc Ca by applying either pressure or temperature is consistent with the transition mechanism proposed by Qiu and Marcus [35]. Based on this work and previous experiments [10,11], the stability region of Ca-I (fcc) is constrained to $0 \leqslant T \leqslant 750$ K and $0 \leqslant P \leqslant 20$ GPa. No evidence of the low-temperature phase reported by Li *et al.* [36] has been found in the present RT and HT experiments.

Over the investigated pressure-temperature (P-T) range, Ca has been observed to undergo two phase transitions, both associated with a coexistence region. Coexistence of Ca-I and Ca-II is observed around 745 K at 3 and 8 GPa during isobaric heating to 800 K. The same coexistence is observed in five different isotherms for $T < 750$ K, and always at a pressure close to 20 GPa (see Fig. 1). In Fig. 2 a selection of integrated XRD patterns obtained during the isobaric ramp at 3 GPa are displayed together with the corresponding azimuthally unwrapped two-dimensional (2D) diffraction images. In this way it is possible to observe the textural and structural evolution of Ca and KCl with increasing temperature. At RT and 3.4 GPa [Figs. 2(a) and 2(b)] Ca-I exhibits a powderlike diffraction pattern, whereas KCl ($B2$ phase) shows some preferred orientation effects. At 728 K additional peaks corresponding to the $B1$ phase of KCl start appearing and the Ca and KCl signals begin showing the formation of some coarse grains [Figs. 2(c) and 2(d)]. At 745 K it is possible to observe the coexistence between Ca-I and the Ca-II phase [Figs. 2(e) and 2(f)]. In this case, both phases present a spotty texture probably due to temperature-induced formation of a large grain microstructure in Ca. The texture of KCl, however, remains unchanged.

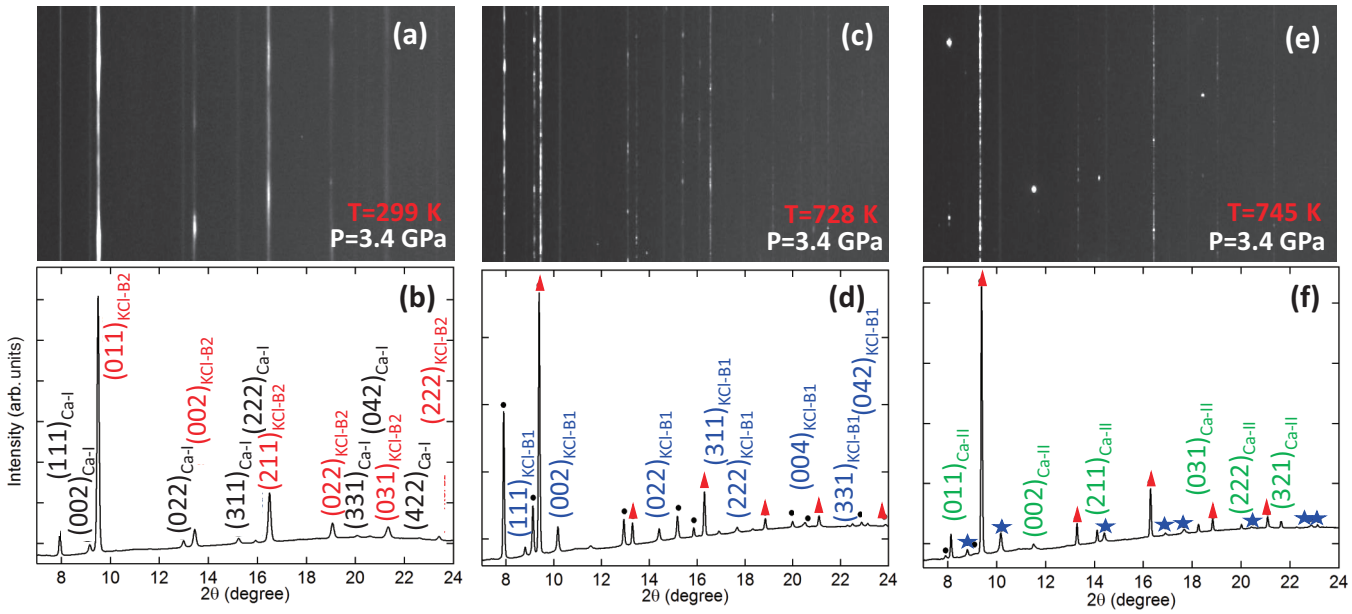

FIG. 2. Azimuthally unwrapped 2D diffraction images (top panel) and corresponding 1D integrated profiles (bottom panel) representing the textural (a), (c), (e) and structural (b), (d), (f) evolution of Ca while increasing the temperature from ambient to 745 K along the 3 GPa isobar. In the integrated diffraction patterns all the reflections are indexed and color coded according to the observed phase. The color code is consistent across (b), (d), (f).

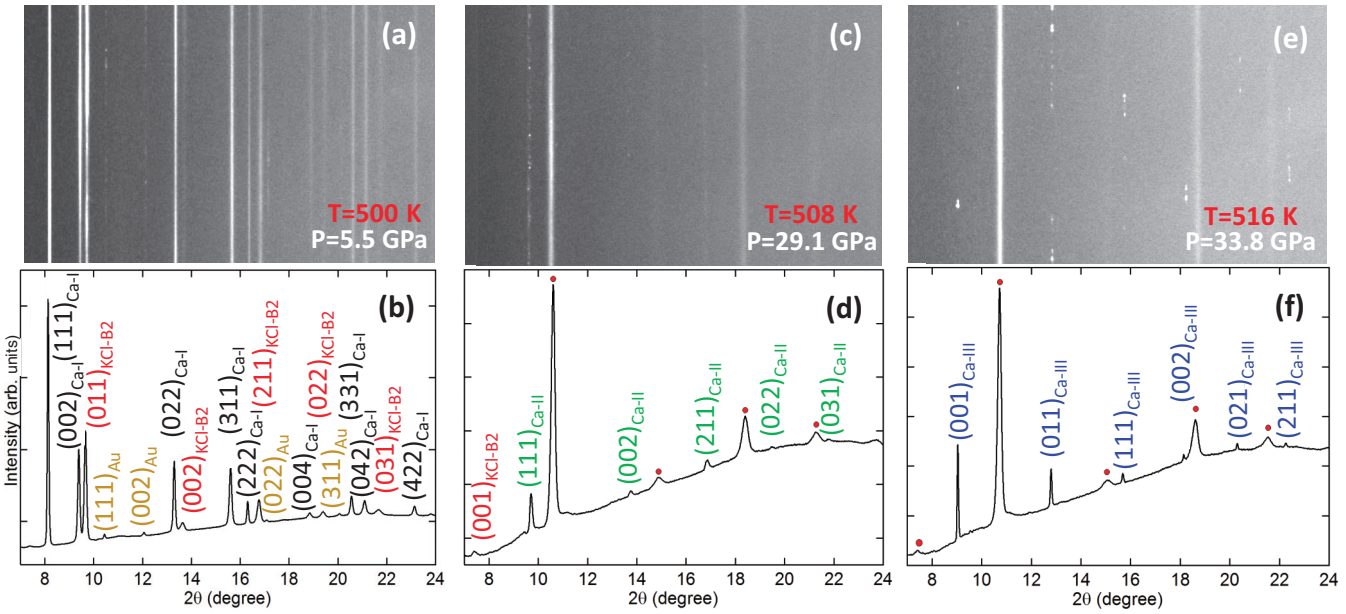

FIG. 3. Azimuthally unwrapped 2D diffraction images (top panel) and corresponding 1D integrated profiles (bottom panel) representing the textural (a), (c), (e) and structural (b), (d), (f) evolution of Ca during the transitions from Ca-I to Ca-II to Ca-III. In the integrated diffraction profiles all the reflections are indexed and color coded according to the observed phase. The color code is consistent across (b), (d), (f). Circles identify peaks from the $B2$ phase of KCl.

An additional phase transition from Ca-II to Ca-III is observed along each of the isotherms investigated in the present study. The existence of this transition excludes the existence of intermediate phases between bcc and sc Ca proposed by Teweldeberhan and Bonev based upon molecular-dynamics simulations [9]. In Fig. 3, the structural evolution of Ca along the ∼500-K isotherm is reported together with the corresponding textural evolution. In this case, low-pressure Ca-I [Figs. 3(a) and 3(b)] transforms to Ca-II, which is illustrated by the results at 508 K and 29.1 GPa [Figs. 3(c) and 3(d)]. It is interesting to observe how, at these P-T conditions, the texture of Ca-II is completely different from that observed during the isobaric temperature ramp where the Ca texture evolves from a powder (Ca-I) into a temperature-induced fine-grain microstructure (Ca-II). Under further compression the crystal structure remains unchanged until 33.8 GPa where a phase transition to the Ca-III phase is observed [Figs. 3(e) and 3(f)]. At these P-T conditions, the KCl reflections show a slight broadening probably due to the stress experienced by the pressure-transmitting medium. The Ca-III XRD patterns instead show an increased orientation of the grains [Fig. 3(f)].

In Fig. 4 the results obtained in the present study are combined with data from previous HP experiments. Our solid-solid phase-boundaries agree well with those reported in a cryogenic HP XRD experiment [36]. The Ca-I-Ca-II phase boundary at around 800 K appears almost horizontal compared to that obtained from calorimetry and resistance measurements [18]. The results are also in good agreement with the phase diagram drawn in a previous melting experiment [19]. In fact, by extrapolating the obtained phase boundaries to higher temperatures, it is possible to observe how the flattening of the melting line and the subsequent dramatic change in the melting line slope around 32 GPa can be associated with the presence of the bcc phase and with a bcc-sc-liquid triple point, respectively, as suggested by Errandonea *et al.* [19].

B. Room-temperature compression and equation of state

Room-temperature compression of Ca was performed up to 53 GPa. In order to obtain results coherent with the entire phase diagram characterization, a sample loading identical to the one used for the resistive-heated DAC was used: a small piece of Ca embedded in KCl. The pressure was determined from the volumetric compression of KCl according to the EOS of Dewaele *et al.* [30] and the results are reported in Fig. 5.

During compression, Ca was observed to undergo two phase transitions: from fcc Ca-I to bcc Ca-II and then to sc Ca-III

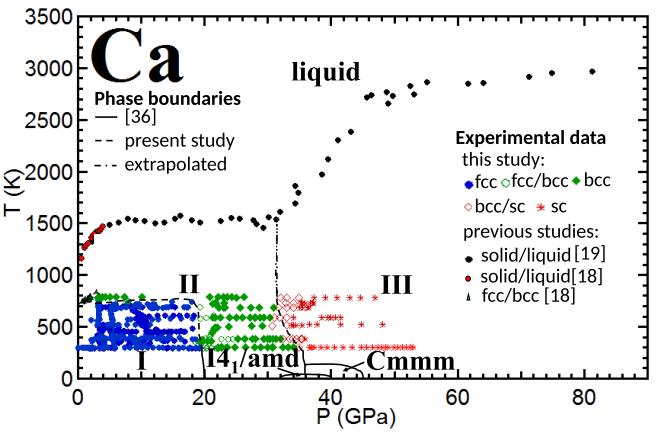

FIG. 4. Phase diagram of Ca comparing the present results with those obtained in previous studies [18,19]. Experimental points are represented with different symbols whereas solid-solid phase boundaries are represented by lines.

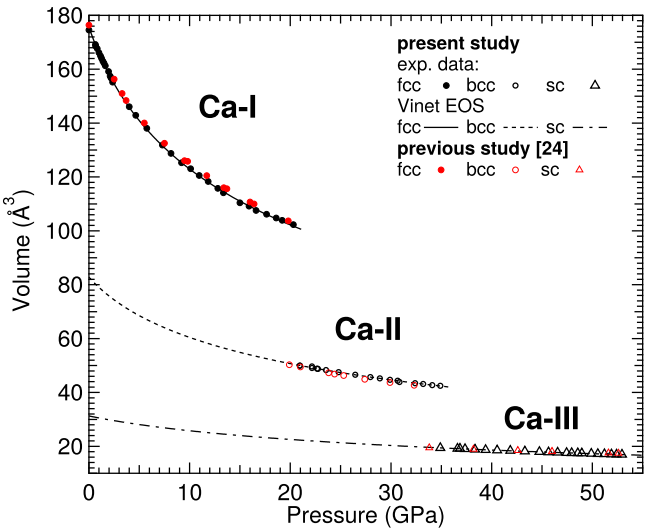

FIG. 5. The compression curve of calcium, as measured at ambient temperature in a KCl pressure medium. Black symbols correspond to the present study while red symbols show data from the previous study by Gu *et al.* [24]. In both cases, different symbols correspond to the different phase observed: Ca-I (closed circle), Ca-II (open circle), and Ca-III (open triangle). Black lines (extrapolated to ambient pressure in the case of Ca-II and Ca-III) represent a fit of the experimental data with a Vinet EOS.

as previously reported in other studies [10,24]. On pressure increase, diffraction peaks from bcc Ca-II were first observed to coexist with fcc Ca-I at 20.3 GPa. The relative change of the volume (normalized per formula unit) at the transition $\Delta V/V_0$ (where V_0 corresponds to the volume at ambient pressure) is determined to be 2.98%. At 22.2 GPa Ca-II becomes the only phase observed and the situation remains the same until 34.9 GPa when peaks from sc Ca-III start to coexist with Ca-II. The volume change at the transition is 11.3%. Finally, at 36.6 GPa, Ca-III is the only phase observed up to 53 GPa, the maximum pressure reached in the present study.

In a previous study, RT EOSs were reported for the Ca-I (fcc), Ca-II (bcc), and Ca-III (sc) phases of Ca [24]. However, very unrealistic values were obtained for the HP phases of Ca. In particular, changes of more than 100% were reported for the bulk modulus at the phase transitions ($K_0 = 17.4,\ 51.9$, and 165 GPa for Ca-I, Ca-II, and Ca-III, respectively). This is unrealistic for a simple metal like Ca and is in contradiction with density-functional-theory calculations [25]. In addition, the previously reported EOS for the Ca-II and Ca-III phases does not properly reproduce the experimental results [25]. As we will explain next, the overestimation of the bulk modulus for bcc and sc Ca can be caused by an underestimation of the volume at ambient pressure of both phases, which unfortunately is not reported by Gu *et al.* [24].

The compression curves of the Ca-I, Ca-II, and Ca-III phases were (individually) fitted with Vinet [37] and third-order Birch-Murnaghan (BM3) EOSs [38] by using the EOSFIT7 package [39]. V_0 of the Ca-I phase was fixed at the experimentally determined value of 175.6(3) Å^3. Determining the value of V_0 for the high-pressure Ca-II and Ca-III phases represents a challenging problem. These phases are not stable

TABLE I. EOS parameters of Ca as obtained in this experiment and in the study of Gu *et al.* [24]. The zero pressure volume V_0, bulk modulus K_0, and its pressure derivative K_0' are listed. The EOS formulations are specified.

	This study Vinet	This study BM3[a]	Gu *et al.* [24] Reported BM3	Gu *et al.* [24] This study BM3
		Ca-I		
V_0 (Å^3)	175.4(3)	175.6(3)		176.2(3)
K_0 (GPa)	16.4(3)	16.0(3)	17.4(5)	16.9(3)
K_0'	3.20(8)	3.32(4)	3.22(4)	3.27(4)
		Ca-II		
V_0 (Å^3)	83.11[b]	83.11(4)		83.11[b]
K_0 (GPa)	18.9(3)	18.3(2)	51.9(3.4)	18.6(5)
K_0'	3.22(6)	3.37(2)	4.2(6)	3.22(5)
		Ca-III		
V_0 (Å^3)	31.279[b]	31.279(14)		31.279[b]
K_0 (GPa)	40(1)	36.7(7)	165.2(4.7)	27(2)
K_0'	2.6(1)	3.17(4)	1.0(3)	4.1(2)

[a]BM3: third-order Birch-Murnaghan.
[b]Fixed values.

at ambient pressure and refining a value for the two V_0 values within EOSFIT7 showed that the parameters were correlated with both K_0 and K_0' at more than 98%. From the BM3 fit the value for the V_0 of the Ca-II phase was found to be 83.11(4) Å^3 whereas for the Ca-III phase the value was 31.279(14) Å^3. In the fits, the starting values for V_0 were obtained by applying the volume changes measured at RT between the Ca-I and Ca-II phases and the Ca-II and Ca-III phases to the V_0 measured for Ca-I. The V_0 value obtained after the fit for the Ca-II phase is consistent with that reported in a previous HT experiment, 89.915 Å^3 at 740 K [41]. The EOS fitted by us for the Ca-II and Ca-III structure reproduce quite well the volume change for the Ca-II/Ca-III transition found here and also reported by Olijnyk and Holzapfel [10]. The present V_0 values were then fixed during the fitting procedure with the Vinet EOS to obtain the bulk modulus (K_0) and its first pressure derivative (K_0'). The results are reported in Table I. In addition, we present the results previously reported by Gu *et al.* [24] and our analysis of their data.

C. Thermal equation of state

From the P-V-T data obtained for the Ca-I and Ca-II phases, it was possible to determine a thermal EOS using the EOSFIT7 package. In general, the experimental data were scattered as a function of temperature; therefore groups of temperature were defined in a range of ±10 K. For the Ca-I phase diffraction data at 298(2), 390(10), 470(20), and 600(20) K were used. During the fitting procedure, the third-order Birch-Murnaghan EOS generated from the RT compression experiment was used as the isothermal part of the P-V-T EOS. A Berman equation [Eq. (1)] was used as the thermal expansion model, assuming a linear variation of K_0 with the temperature, as described in Angel *et al.* [39]:

$$V_{0T} = V_{00}\left(1 + \alpha_0(T - T_{\mathrm{ref}}) + \tfrac{1}{2}\alpha_1(T - T_{\mathrm{ref}})^2\right). \quad (1)$$

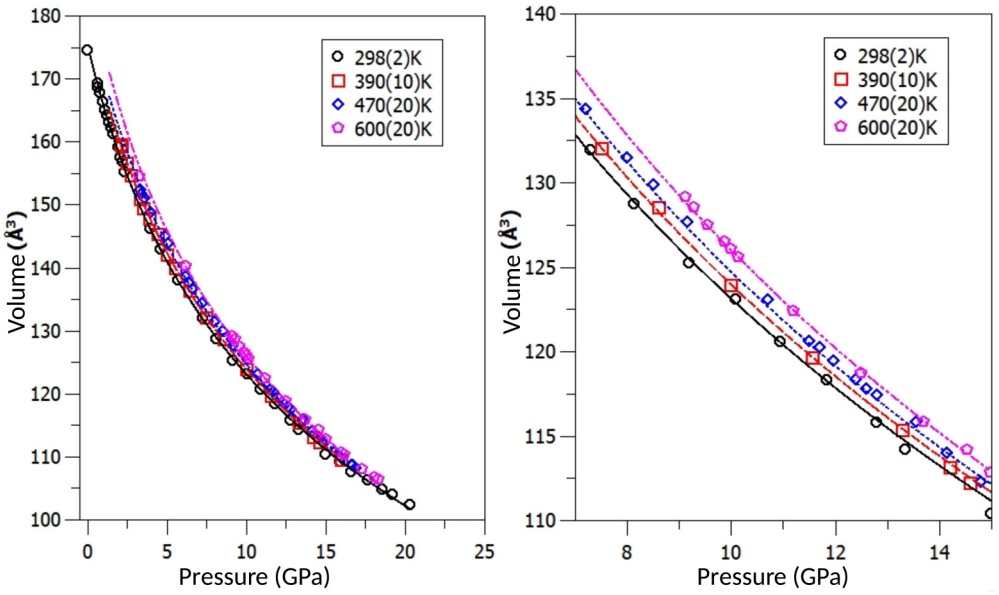

FIG. 6. (a) Pressure-volume curves of Ca-II obtained by grouping data according to temperatures (see text). (b) Expanded view of 7–15-GPa data. The symbols represent different temperature groups whereas the lines represent the corresponding P-V-T EOS fit.

In the Berman equation V_{0T} and V_{00} represent, respectively, the volume at T_{ref} (298 K in this case) and the volume at the measured T. α_0 and α_1 are the two terms of the expansion of the thermal coefficient $[\alpha(T)]$ as proposed by Berman: $\alpha(T) \sim \alpha_0 + \alpha_1(T - T_{\text{ref}})$. α_0 is the thermal expansion coefficient at T_{ref}.

In Fig. 6 the experimental data are shown together with the corresponding P-V-T EOS. The results are reported in Table II. The values of α_0 and α_1 are on the same order of magnitude of those reported for Mg [41].

A procedure identical to the one used for Ca-I was used to characterize the P-V-T EOS of Ca-II. In this case, though, different groups of temperatures were defined: 298(2), 480(20), 585(5), and 785(10) K. However, little difference was observed between the data at 480 and 585 K so the data at 480 K was not used. This little difference is due to the small thermal expansion of Ca-II (see Table II). As a consequence of it, a 100-K change will produce a volumetric change comparable to the experimental accuracy and data scattering. In Fig 7, the curves obtained are represented and the fitting results are reported in Table II. It is clear from Figs. 6 and 7 that the EOSs obtained are in good agreement with the experimental data. The results for Ca-II are consistent with earlier results [40] at ambient pressure and HT (see the data point at 740 K).

TABLE II. P-V-T EOS parameters generated in the present study using a BM3 and a Berman model for the Ca-I and the Ca-II phases.

	Ca-I	Ca-II
V_0 (Å^3)	175.6(3)	83.11(4)
K_0 (GPa)	16.0(3)	18.3(2)
K_0'	3.32(4)	3.37(2)
dK/dT (GPa/K)	−0.0079(5)	−0.0094(7)
$\alpha_0(K^{-1})$ $(\times 10^{-5})$	18.4(9)	16(3)
$\alpha_1(K^{-2})$ $(\times 10^{-8})$	17(6)	72(10)

However, the fits reproduce more accurately the experimental results for the Ca-I than for the Ca-II phase.

The accurate description given by the Berman model to the results of the Ca-I (fcc) phase suggests that this model can be successfully applied to other metals with a HP-HT

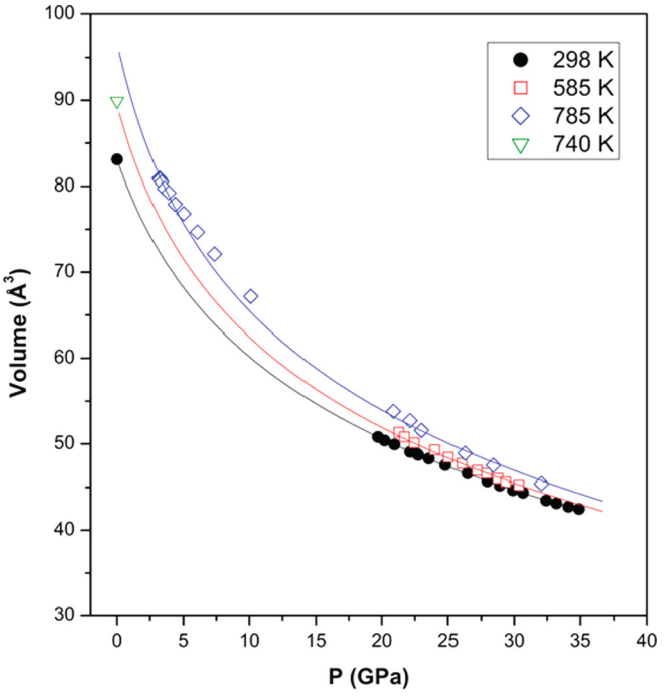

FIG. 7. Pressure-volume curves of Ca-II obtained by grouping data according to temperatures (see text). The symbols represent different temperature groups whereas the lines represent the corresponding P-V-T EOS fit. The same color code has been used for experiments and fits. One data point taken from the literature [33] is included for $T = 740$ K and ambient pressure.

fcc phase, such as palladium and platinum [42]. In the case of Ca-II (bcc), a very good agreement can be observed between the experimental data and the EOS obtained for the temperature groups at 298 and 585 K. Regarding the group at 785 K, the experimental data do not seem to agree very well with the obtained EOS, particularly in the low-pressure region where there is a non-negligible misfit. A reason for this can be the contribution of anharmonic effects not considered in the model which become less important as pressure increases. Indeed, in other metals the bcc phase has been found to be strongly anharmonic [43]. However, under compression, as the volume goes down, the anharmonic corrections decrease by almost one-half [43]. This is the reason why there is a large misfit in the P-V-T EOS at 785 K.

IV. CONCLUSIONS

In the present study, the phase diagram of Ca has been investigated using resistively heated DACs and AD-XRD from ambient conditions up to 53 GPa and 800 K. This systematic study allows the determination of accurate phase boundaries for the different solid-solid phase transitions of Ca, which are found to be in good agreement with those reported in previous high-pressure experiments [10,17–19]. The present characterization of the Ca phase diagram links the two Ca-II (bcc) phases observed at low pressure and high temperature and at ambient temperature and high pressure, and confirms the connection between the bcc phase and the flat melting curve observed up to 32 GPa. Our study has also allowed the characterization of the Ca-III (sc) phase at high P-T conditions. Furthermore, the present study has corrected the previously reported RT EOS for the Ca-II (bcc) and Ca-III (sc) phases. Finally, the RT compression curve of Ca up to 53 GPa has enabled the characterization of the P-V-T EOS of the Ca-I (fcc) and Ca-II (bcc) phases of Ca using a Berman model assuming a linear variation of the bulk modulus as a function of temperature. However, a large part of the P-T phase diagram remains unexplored and further experiments are necessary to extend our knowledge of this system.

ACKNOWLEDGMENTS

The authors acknowledge the ALBA and DLS synchrotron facilities for provision of beamtime on the beamlines MSPD and I15, respectively (DLS Proposal No. EE15864). ©British Crown Owned Copyright 2018/AWE. Published with permission of the Controller of Her Britannic Majesty's Stationery Office. Part of the research was supported by the Spanish Government MINECO under Grants No. MAT2016-75586-C4-1/4P and No. MAT2015-71070-REDC. M.I.M. is grateful to AWE for the award of a William Penney Fellowship.

[1] C. Klein and C. S. Hurlbut Jr., *Manual of Mineralogy*, 20th ed. (John Wiley, New York, 1985), p. 329.
[2] C. Klein and C. S. Hurlbut Jr., *Manual of Mineralogy*, 20th ed. (John Wiley, New York, 1985), p. 352.
[3] C. Cazorla and D. Errandonea, Phys. Rev. Lett. **113**, 235902 (2014).
[4] W. Owusu W. C. Willett, D. Feskanich, A. Ascherio, D. Spiegelman, and C. A. Colditz, J. Nutr. **127**, 1782 (1997).
[5] F. Pu, N. Chen, and S. Xue, Food Sci. Human Wellness **5**, 8 (2016).
[6] C. R. Ropp, *Encyclopedia of the Alkaline Earth Compounds* (Elsevier, Amsterdam, 2013), pp. 12–15.
[7] H. L. Skriver, Phys. Rev. Lett. **49**, 1768 (1982).
[8] R. Ahuja, O. Eriksson, J. M. Wills, and B. Johansson, Phys. Rev. Lett. **75**, 3473 (1995).
[9] A. M. Teweldeberhan and S. A. Bonev, Phys. Rev. B **78**, 140101(R) (2008).
[10] H. Olijnyk and W. B. Holzapfel, Phys. Lett. A **100**, 191 (1984).
[11] T. Yabuuchi, Y. Nakamoto, K. Shimizu, and T. Kikegawa, J. Phys. Soc. Jpn. **74**, 2391 (2005).
[12] T. Ishikawa, A. Ichikawa, H. Nagara, M. Geshi, K. Kusakabe, and N. Suzuki, Phys. Rev. B **77**, 020101 (2008).
[13] H. Fujihisa, Y. Nakamoto, K. Shimizu, T. Yabuuchi, and Y. Gotoh, Phys. Rev. Lett. **101**, 095503 (2008).
[14] Y. Nakamoto, M. Sakata, K. Shimizu, H. Fujihisa, T. Matsuoka, Y. Ohishi, and T. Kikegawa, Phys. Rev. B **81**, 140106 (2010).
[15] M. Sakata, Y. Nakamoto, K. Shimizu, T. Matsuoko, and Y. Ohishi, Phys. Rev. B **83**, 220512(R) (2011).
[16] H. Fujihisa, Y. Nakamoto, M. Sakata, K. Shimizu, T. Matsuoka, Y. Ohishi, H. Yamawaki, S. Takeya, and Y. Gotoh, Phys. Rev. Lett. **110**, 235501 (2013).
[17] G. C. Kennedy and R. C. Newton, *Solids Under Pressure* (McGraw-Hill, New York, 1963).
[18] A. Jayaraman, W. Klement Jr., and G. C. Kennedy, Phys. Rev. **132**, 1620 (1963).
[19] D. Errandonea, R. Boehler, and M. Ross, Phys. Rev. B **65**, 012108 (2001).
[20] H. K. Mao, J. Xu, and P. M. Bell, J. Geophys. Res. **91**, 4673 (1986).
[21] D. Errandonea, J. Phys. Chem. Solids **67**, 2017 (2006).
[22] R. Boehler, Earth Planet. Sci. Lett. **111**, 217 (1992).
[23] R. Boehler, Phys. Earth Planet. Inter. **96**, 181 (1996).
[24] Q. F. Gu, G. Krauss, Y. Grin, and W. Steurer, Phys. Rev. B **79**, 134121 (2009).
[25] F. Jona and P. M. Marcus, J. Phys.: Condens. Matter **18**, 4623 (2006).
[26] F. Fauth, I. Peral, C. Popescu, and M. Knapp, Powder Diffr. **28**, S360 (2013).
[27] C. Cazorla, S. G. MacLeod, D. Errandonea, K. A. Munro, M. I. McMahon, and C. Popescu, J. Phys.: Condens. Matter **28**, 445401 (2016).
[28] G. W. Stinton, S. G. MacLeod, H. Cynn, D. Errandonea, W. J. Evans, J. E. Proctor, Y. Meng, and M. I. McMahon, Phys. Rev. B **90**, 134105 (2014).
[29] P. I. Dorogokupets and A. Dewaele, High Press. Res. **27**, 431 (2007).
[30] A. Dewaele, A. B. Belonoshko, G. Garbarino, F. Occelli, P. Bouvier, M. Hanfland, and M. Mezouar, Phys. Rev. B **85**, 214105 (2012).
[31] C. Prescher and V. B. Prakapenka, High Press. Res. **35**, 223 (2015).

[32] A. A. Coelho, TOPAS-Academic Version 4.1. Computer Software (TOPAS-Academic, Coelho Software, Brisbane, 2007).
[33] D. Errandonea, O. Gomis, D. Santamaria-Perez, B. Garcia-Domene, A. Munoz, P. Rodriguez-Hernandez, S. N. Achary, A. K. Tyagi, and C. Popescu, J. Appl. Phys. **117**, 105902 (2015).
[34] A. J. Bray, Adv. Phys. **43**, 357 (1994).
[35] S. L. Qiu and P. M. Marcus, Eur. Phys. J. B **86**, 425 (2013).
[36] B. Li, Y. Ding, W. Yang, L. Wang, B. Zou, J. Shu, S. Sinogeikin, C. Park, G. Zou, and H. K. Mao, Proc. Natl. Acad. Sci. USA **109**, 16459 (2012).
[37] P. Vinet, J. Ferrante, J. H. Rose, and J. R. Smith, Geophys. Res. **92**, 9319 (1987).
[38] R. Angel, in *High-Temperature and High-Pressure Crystal Chemistry*, Reviews in Mineralogy and Geochemistry Vol. 41 (Mineralogical Society of America, Washington, D.C., 2000), pp. 35–59.
[39] R. J. Angel, M. Alvaro, and J. Gonzalez-Platas, Z. Kristallogr. **229**, 405 (2014).
[40] B. T. Bernstein and J. F. Smith, Acta Crystallogr. **12**, 419 (1959).
[41] D. Errandonea, Y. Meng, D. Häusermann, and T. Uchida, J. Phys.: Condens. Matter **15**, 1277 (2003).
[42] D. Errandonea, Phys. Rev. B **87**, 054108 (2013).
[43] V. Yu. Trubitsin and E. B. Dolgusheva, Phys. Rev. B **76**, 024308 (2007).